



# A nomogram based on a combination of preoperative multimodal imaging and serological signatures for predicting microvascular invasion of hepatocellular carcinoma: an independent external validation study

Jie Wu<sup>1#</sup>, Yadan Xu<sup>2#</sup>, Han Liu<sup>1</sup>, Baojie Wen<sup>1</sup>, Wenping Wang<sup>2\*</sup>, Wentao Kong<sup>1\*</sup>

<sup>1</sup>Department of Ultrasound, Nanjing Drum Tower Hospital, Affiliated Hospital of Medical School, Nanjing University, Nanjing, China;

<sup>2</sup>Department of Ultrasound, Zhongshan Hospital, Fudan University, Shanghai, China

**Contributions:** (I) Conception and design: W Wang, W Kong; (II) Administrative support: W Wang, W Kong; (III) Provision of study materials or patients: B Wen, H Liu; (IV) Collection and assembly of data: Y Xu, B Wen, H Liu; (V) Data analysis and interpretation: J Wu, Y Xu; (VI) Manuscript writing: All authors; (VII) Final approval of manuscript: All authors.

<sup>#</sup>These authors contributed equally to this work as co-first authors.

<sup>\*</sup>These authors contributed equally to this work as co-corresponding authors.

**Correspondence to:** Wenping Wang, PhD. Department of Ultrasound, Zhongshan Hospital, Fudan University, 180 Fenglin Road, Shanghai 200032, China. Email: puguang61@126.com; Wentao Kong, PhD. Department of Ultrasound, Nanjing Drum Tower Hospital, Affiliated Hospital of Medical School, Nanjing University, 321 Zhongshan Road, Nanjing 210003, China. Email: breezewen@163.com.

**Background:** Microvascular invasion (MVI) is a key determinant of recurrence and survival in hepatocellular carcinoma (HCC), yet it remains difficult to assess preoperatively. Robust, noninvasive tools integrating multimodal imaging and serological features are needed to inform surgical planning. This study aimed to establish and validate a reliable diagnostic model based on a combination of multimodal imaging and serological signatures for predicting MVI in HCC.

**Methods:** This retrospective study included 179 patients with HCC treated at the Nanjing Drum Tower Hospital, Affiliated Hospital of Medical School, Nanjing University, from 2015 to 2022. Univariable logistic regression was used for initial screening; variables with  $P < 0.10$  entered the multivariable logistic regression with backward stepwise selection. A nomogram was then constructed and internally (bootstrap) and externally validated to investigate the associations of MVI features based on multimodal imaging and serological signatures. A nomogram was developed and was externally validated in an independent cohort from Zhongshan Hospital, Fudan University (Institution 2) ( $n=80$ ).

**Results:** Logistic regression analysis was performed to identify seven parameters related to MVI, including tumor number, diameter, Adler blood flow grading, visualized macrovascular around the tumor, arterial peritumoral enhancement, nonenhancing area, and non-nodular type tumor. Based on these seven parameters, a final combined model was developed. The accuracy, sensitivity, specificity, positive predictive value, and negative predictive value in predicting MVI were 88.0% and 84.0%, 72% and 84.0%, 94.0% and 84.0%, 81.0% and 82.0%, 91% and 86.0% in the modeling and validation cohorts, respectively.

**Conclusions:** A reliable combined model based on multimodal imaging and serological signatures effectively predicts preoperative MVI in patients with HCC and may assist clinicians in determining the

<sup>^</sup> ORCID: 0000-0002-3483-7736.

optimal intervention and achieving greater precision and individualization of treatment.

**Keywords:** Hepatocellular carcinoma (HCC); microvascular invasion (MVI); ultrasound; magnetic resonance imaging (MRI); nomogram

Submitted Feb 01, 2025. Accepted for publication Aug 26, 2025. Published online Oct 21, 2025.

doi: 10.21037/qims-2025-231

View this article at: <https://dx.doi.org/10.21037/qims-2025-231>

## Introduction

Hepatocellular carcinoma (HCC), the most common malignant liver tumor in the world, is widely known for its rising morbidity and mortality (1). The mainstay treatment for HCC is surgical resection (2); however, the 5-year survival rate remains poor due to the spread, metastases, and high recurrence rate of HCC (3).

The presence of microvascular invasion (MVI), a significant pathogenic component, is a high-risk indicator of HCC relapse and early mortality and is associated with decreased long-term patient survival (4-6). The majority of MVIs occur within 1 cm of the tumor site. Wider surgical margins contribute to the radical treatment of HCC and increase the total survival rate of these patients (7,8). MVI-positive patients with surgical margins <1 cm have an almost two-times greater risk of early recurrence and death as compared to those with margins >1 cm (9). Consequently, if MVI is positive, patients require wider surgical or ablation margins, and a liver transplant should also be considered an alternative treatment. However, MVI can only be definitively detected by postoperative pathology, but an adequate, uniform standard for the preoperative prediction of MVI in patients with HCC appears to be lacking (10).

Numerous studies have evaluated certain serological signatures as predictive factors. The results of these studies suggest that the aggressive biological behaviors of HCC may contribute to the presence of MVI (5,11,12). Several novel potential biomarkers, such as inflammatory biomarkers, have also been associated with predicting MVI. Preoperative platelet-to-lymphocyte ratio (PLR) and neutrophil-to-lymphocyte ratio (NLR) are significant independent risk factors for MVI (11). However, it should be noted that a few serological signatures have varying degrees of abnormality in diseases such as chronic hepatitis and cirrhosis. For prediction to be accurate, this factor must be considered.

Research has also indicated that preoperative imaging can be used to predict MVI in patients with HCC. Imaging

tools, including computed tomography (CT), magnetic resonance imaging (MRI), and ultrasound, are critical to determining the tumor size, number, and morphology. They can also provide information on tumor margin, capsule, arterial peritumoral enhancement, and intratumor artery condition. Accordingly, imaging constitutes a key component of noninvasive MVI risk stratification and model development in the preoperative setting (13-17).

Several international guidelines recommend conventional ultrasound (CUS) as the first-line screening tool for high-risk HCC populations, due to its real-time, noninvasive, low-cost, and radiation-free nature (18). With contrast-enhanced ultrasound (CEUS), tumor microvascular perfusion can also be dynamically evaluated. Previous studies have shown that CEUS-based quantitative perfusion analysis can help differentiate malignant tumors and predict MVI in HCC (17,19). Compared with MRI, CEUS has demonstrated high sensitivity and strong agreement with histopathology, supporting its diagnostic value in HCC (20). However, CEUS uses purely intravascular microbubble agents, whose pharmacokinetics and quantitative reproducibility differ substantially from CT and MRI, limiting direct cross-modality comparability (21). In addition, CUS remains highly operator-dependent and sensitive to equipment variability. Given these considerations, our study focused on robust qualitative CEUS features (such as non-enhancing areas or peritumoral enhancement), which are less affected by inter-operator and inter-platform variability, while MRI features (e.g., nonsmooth tumor margins, arterial rim or peritumoral enhancement) have also been widely reported as predictors of MVI (15,22).

Previous studies on MVI have largely focused on only a single imaging characteristic, and, to our knowledge, an analysis of the combination of multiple imaging features for predicting MVI is lacking.

Accordingly, we conducted a study to examine the association of CUS, CEUS, and MRI features with the incidence of MVI in patients with HCC. We further

developed and validated a preoperative prediction nomogram, incorporating the multimodal imaging features and serological signatures for the preoperative prediction of MVI. We hope that the preoperative, noninvasive evaluation offered by our model can assist clinicians in optimizing treatment. We present this article in accordance with the TRIPOD reporting checklist (available at <https://qims.amegroups.com/article/view/10.21037/qims-2025-231/rc>).

## Methods

### Patients

As part of this study, the clinical data of 521 patients with suspected HCC treated at the Nanjing Drum Tower Hospital, Affiliated Hospital of Medical School, Nanjing University (institution 1), and Zhongshan Hospital, Fudan University (institution 2), treated from October 2015 to December 2022, were retrospectively analyzed.

This following inclusion criteria were applied: (I) tumor resection or liver transplantation, (II) a histopathological diagnosis of HCC with confirmation of MVI-positive or MVI-negative status, (III) no previous treatment for HCC (e.g., hepatectomy, liver transplantation, chemotherapy, radiotherapy, and immunosuppressive therapy), (IV) no extrahepatic metastasis, (V) Child-Pugh liver function class A or B, and (VI) availability of multimodal image data (including CUS and CEUS examinations performed within the 2 weeks before surgery and MRI within 1 month before surgery). Meanwhile, the exclusion criteria included (I) nonprimary liver cancer or combination with other types of tumors, (II) administration of antitumor therapy before surgery, and (III) incomplete imaging data or missing clinicopathological data.

### Modeling cohort

Ultimately, 259 patients with HCC (38 women and 221 men; age range 23–82 years) were included in this study. The final modeling cohort based on institution 1 contained 179 patients, and their data are summarized in [Table S1](#). Ethical approval was obtained from the Institutional Review Board of Nanjing Drum Tower Hospital, Affiliated Hospital of Medical School, Nanjing University (Approval No. 2022-140-01), which waived the requirement for informed consent owing to the retrospective nature of the analysis. Zhongshan Hospital, Fudan University, was informed of and agreed to the study in accordance with institutional

policy. This study was conducted in accordance with the Declaration of Helsinki and its subsequent amendments.

### Validation cohort

We validated the performance of this model with an independent external cohort of 80 patients with HCC from institution 2, whose data were retrospectively analyzed. The inclusion and exclusion criteria were the same as those for the modeling cohort. The flowchart of cohort construction is included in *Figure 1*.

A formal sample size calculation was not performed. Rather, the study size was determined by the number of eligible patients with complete preoperative imaging and postoperative pathological MVI status during the study period.

### Multimodal imaging acquisition

#### CUS

Within 2 weeks before surgery, a standard liver ultrasound examination was performed with a LogicE9 ultrasound machine (GE HealthCare, Chicago, IL, USA) equipped with a convex array probe frequency of 2–5 MHz. Lesions were initially investigated for their location, size, and morphology. For patients with multinodular HCC, the lesion with the largest diameter was considered the target lesion for further analysis. For each lesion, gain, depth, and focus were optimized to attain the best section. The largest lesion segment without a blind spot was examined.

#### CEUS

After the location of the lesion was ascertained via CUS, the most apparent section was selected, and the position was fixed. The contrast-enhancing agent (2.4 mL; SonoVue, Bracco, Milan, Italy) was injected into the antecubital vein immediately before scanning and was followed by flushing with 5 mL of 0.9% normal saline solution. Continuous monitoring of target lesion was commenced immediately at the same time of the injection. For each patient, at least 4 minutes of digital video were continually recorded and saved to a hard disk, and all the captured images were converted to Digital Imaging and Communications in Medicine (DICOM) format for analysis. After intravenous injection of the contrast, images of the arterial phase, portal venous phase, and delayed phase were acquired at 0–30 s, 31–120 s, and 12–240 s, respectively.

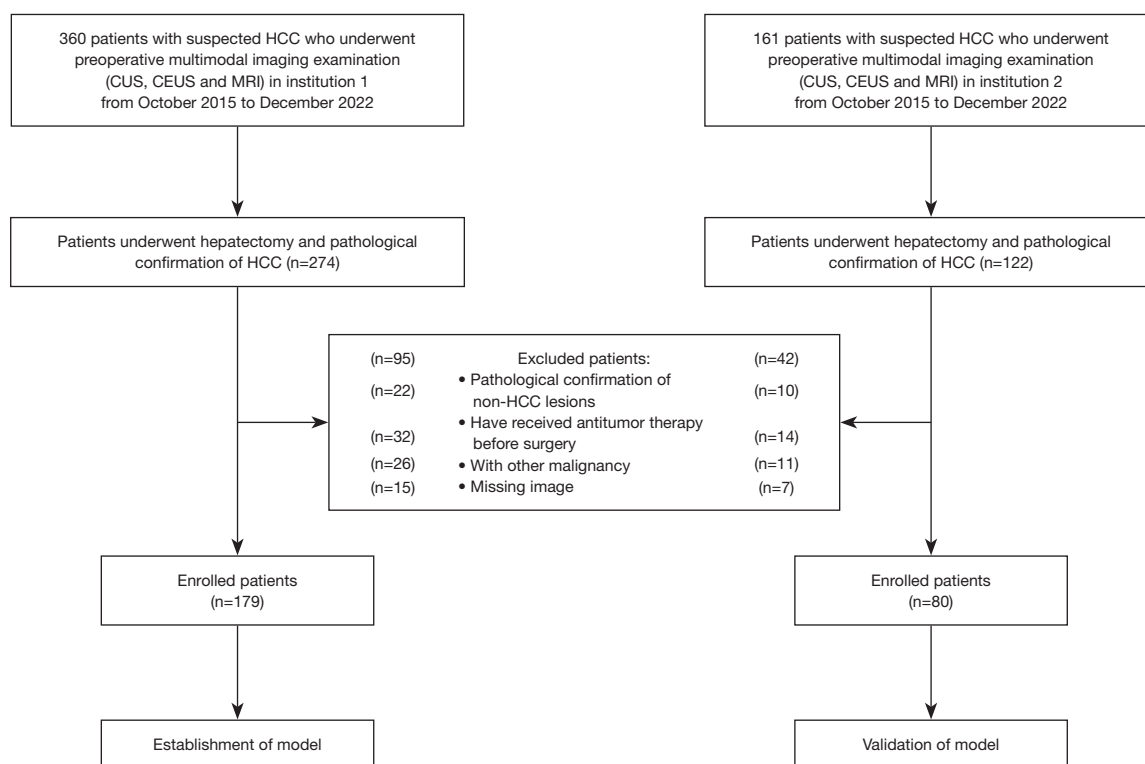


**Figure 1** Flowchart of patient enrollment. The inclusion and exclusion process are separately illustrated for modeling cohort from institution 1 (Nanjing Drum Tower Hospital, Affiliated Hospital of Medical School, Nanjing University) and the validation cohort of institution 2 (Zhongshan Hospital, Fudan University). CEUS, contrast-enhanced ultrasound; CUS, conventional ultrasound; HCC, hepatocellular carcinoma; MRI, magnetic resonance imaging.

## MRI

Patients underwent scanning with a 1.5-T or 3.0-T MRI Achieva device (Philips Healthcare, Amsterdam, the Netherlands) with an eight-channel phased array coil within 1 month before surgery. For the MRI sequences, a power injector (Bayer, Leverkusen, Germany) was used to inject gadopentetate dimeglumine (Magnevist; Bayer) at 2 mL/s and a speed of 0.1 mmol/kg body weight. Radiologists reviewed images obtained in the early arterial phase, late arterial phase, portal vein phase, and delayed phase.

Both institution 1 and 2 followed standardized imaging acquisition protocols, using identical ultrasound and MRI scanner models, as well as consistent contrast agent administration parameters, to ensure the comparability of imaging features and data quality across the two cohorts.

## Imaging analysis

Radiologists with 6 and 10 years of experience in liver imaging independently evaluated the MRI results, and two radiologists with more than 10 years of experience reviewed

all available CUS and CEUS studies. All radiologists were blinded to the clinical and pathological data of the patients.

All imaging features were visually assessed by two radiologists independently, and any disagreements were resolved by discussion. Cohen's kappa statistics were used to assess interobserver agreement on key features included in the final model. The  $\kappa$  values ranged from 0.78 to 0.88, indicating substantial to excellent agreement.

## Nonenhanced features

The evaluation of nonenhanced features was as follows (Figures S1,S2). (I) Tumor location was categorized as right lobe, left lobe, caudate lobe, or crossing the right and left lobes. (II) Tumor number was categorized as solitary ( $n=1$ ) or multiple ( $n>1$ ). (III) Tumor size was defined as the maximal diameter of the lesion on multimodal imaging. (IV) Tumor shape on CUS was categorized as regular shape (defined as a nodular tumor; Figure S1A) or irregular shape (defined as focal extranodular extension, multinodular confluence, and focal infiltrative margin; Figure S1B-S1D).

Tumor shape on MRI was categorized as nodular (defined as round or round-like nodules with clear and regular borders; [Figure S1E](#)) or non-nodular (defined as protruding, multiple fused nodules, and irregular infiltration; [Figure S1F-S1H](#)). (V) Tumor margin was categorized as clear or unclear. (VI) Echogenicity was categorized into four states (hyperechoic, isoechoic, hypoechoic, or multiple fused echoes; [Figure S1I-S1L](#)) based on the primary echo intensity inside the tumor as compared to that in the adjacent normal liver parenchyma. (VII) Tumor blood flow signal was detected via color Doppler flow imaging (CDFI) and was evaluated according to the Alder grading system of blood flow as follows: grade 0 (absent), no blood flow visualized; grade I (minimal), one- or two-pixels containing flow; grade II (moderate), a main vessel and/or several small vessels; and grade III (marked), four or more vessels ([Figure S2A-S2D](#)) (23). (VIII) Macrovascularity around the tumor on CUS was defined as peripheral prominent portal veins, hepatic vein, or their branches located near (<1 cm) the tumor ([Figure S2E,S2F](#)).

### Enhanced features

#### CEUS

The evaluation of CEUS features was as follows ([Figure S3](#)): (I) the degree of enhancement (hypo-, iso-, hyper-, or mixed enhancement) was determined by comparing tumor lesions with the surrounding liver tissue in the arterial, portal venous, and delayed phases ([Figure S3A-S3D](#)); (II) the enhancement pattern was classified as heterogeneous, homogeneous, or ring-like enhancement ([Figure S3E-S3G](#)); (III) arterial peritumoral enhancement was defined as a detectable portion of hyperenhancement outside the tumor margin with comprehensive contact to the tumor border, followed by isoenhancement with the background liver parenchyma in the delayed phase ([Figure S3H](#)); (IV) capsular enhancement was defined as a peripheral ring of smooth hyperenhancement in the portal venous or delayed phase ([Figure S3I](#)); (V) nonenhancing area was defined as any nonenhanced area inside the tumor; (VI) washout was defined as hypoenhancement in the tumor compared to the surrounding parenchyma; the time and intensity of washout were categorized as early washout (<60s) or marked washout.

#### MRI

The evaluation of MRI features was as follows ([Figure S4](#)). (I) The homogeneity of tumor signal intensity assessed on

transverse T2-weighted imaging (T2-WI) was categorized as homogenous or heterogeneous ([Figure S4A](#)). (II) The enhancement pattern was categorized as early arterial enhancement with early washout, peritumoral enhancement (patchy or crescent-shaped region surrounding the tumor exhibiting arterial phase hyperintensity and portal phase isointensity; [Figure S4B](#)), rim enhancement (annular region of the tumor with increased intensity during the arterial phase; [Figure S4C](#)), or asynchronous enhancement (hyperenhancing and hypoenhancing zones in different parts of the lesion during the same period; [Figure S4D](#)). (III) Pseudocapsule of the tumor was defined as present or absent ([Figure S4E](#)).

### Laboratory indicators

Preoperative laboratory tests included complete liver and renal function tests, including for hepatitis B immunology, hepatitis B surface antigen (HBsAg), serum alpha-fetoprotein (AFP) level, carcinoembryonic antigen (CEA), carbohydrate antigen199 (CA199), carbohydrate antigen125 (CA125), serum alanine aminotransferase (ALT), aspartate aminotransferase (AST),  $\gamma$ -glutamyl transpeptidase (GGT), serum total bilirubin (TB), serum albumin (ALB), alkaline phosphatase (ALP), lymphocyte count (LR), neutrophil count (N), platelet count (PLT), prothrombin time (PT), and serum creatinine (Scr). Other inflammatory indices were derived as follows: the alkaline phosphatase-to-lymphocyte ratio (ALR) was calculated as  $ALR = ALP (U/L) / LR (\times 10^9/L)$ ; the NLR as  $NLR = N (\times 10^9/L) / LR (\times 10^9/L)$ ; and the PLR as  $PLR = PLT (\times 10^9/L) / LR (\times 10^9/L)$ .

### Pathological outcomes

A postoperative histopathological evaluation was performed on resected specimens using hematoxylin-eosin (H&E) staining. MVI was defined as the histopathologic presence of tumor cell clusters within endothelial-lined microvessels in the peritumoral liver parenchyma. For statistical analyses and model development, patients were dichotomized as MVI-positive if >50 intravascular tumor cells were identified and MVI-negative otherwise (24). Two pathologists with at least 10 years' experience in HCC independently reviewed all slides; discrepancies were resolved by consensus or adjudication by a senior pathologist.

### Statistical analysis

R software version 3.6.1 (The R Foundation for Statistical Computing) and SPSS 24.0 (IBM Corp., Armonk, NY,



USA) software were used for all statistical analyses. Normally and nonnormally distributed data are expressed in numbers and percentages for categorical variables and as the mean  $\pm$  SD or median with interquartile range (IQR) for continuous variables, respectively.

Baseline clinical and pathologic factors were compared between the two groups via the Chi-squared test for categorical variables or with the *t*-test for continuous variables, as appropriate.

Firstly, an analysis of predictor variables capable of classifying MVI into positive and negative status was conducted in patients with HCC via univariable logistic regression. Subsequently, stepwise backward elimination was applied to select variables with a *P* value under 0.1 for inclusion in the models (variables with *P* < 0.10 in the univariate logistic regression analysis were entered into the multivariate logistic regression analysis). Based on the corresponding final logistic models, nomograms were constructed to predict these features.

The prediction model was then retested for internal validation via 500 bootstrap replicates. External validation was also conducted to assess any heterogeneity in model performance between the two institutions.

A calibration curve was used to evaluate the model performance in the cohorts. For quantifying the predictive performance, we used the area under the receiver operating characteristic (ROC) curve (AUC) with the 95% confidence interval (CI), accuracy, sensitivity, specificity, positive predictive value (PPV), and negative predictive value (NPV). Finally, we evaluated our model's clinical benefit through decision curve analysis. The threshold for statistical significance was a two-sided *P* = 0.1. There were no missing data for the variables included in the model. Therefore, a complete case analysis was performed.

For prespecified benchmarking, we fitted an extra model composed of variables frequently reported as worrisome predictors of MVI in HCC—AFP, tumor number, tumor diameter, arterial peritumoral enhancement, and non-nodular tumor type. The extra model used the same multivariable logistic framework and backward stepwise selection criteria as the main analyses. Model performance was assessed in both the modeling and external validation cohorts using discrimination (ROC AUC with 95% CI), calibration (bootstrap-corrected calibration curves), and clinical utility [decision-curve analysis (DCA)].

## Results

### Demographics

The modeling cohort (institution 1) included 179 patients. The patients' mean age was 60 years (IQR 51–66 years), there were 149 (83.2%) men and 30 (16.8%) women, and MVI was present in 26.3% (47/179) of the patients. The external validation cohort (institution 2) included 80 patients. The mean age of the patients was 60 years (IQR 53–67 years), there were 72 (90%) men and 8 (10%) women, and MVI was present in 46.3% (37/80) of the patients (Table S1).

### Clinical features associated with MVI in univariate and multivariate analyses

According to univariate analyses, several variables, including sex, age, pathological type, PLR, ALT, AST, GGT, tumor number, diameter, capsule, Adler blood flow grading, visualized macrovascular around the tumor, arterial peritumoral enhancement, nonenhancing area, marked washout, non-nodular type tumor, and signal intensity, were associated with MVI (all *P* values < 0.1).

Specifically, 64 lesions (24.71%) presented with nonenhancing components on CEUS. This feature was analyzed as a binary variable (present or absent) and remained significant in the multivariate analysis of the combined model.

In the multivariable analyses, we fitted three logistic prediction models using backward stepwise selection, with imaging information added sequentially from CUS to CEUS to MRI. Candidate predictors at each step included prespecified serological indices and imaging features from the relevant modalities; variables were retained only if selected by the stepwise procedure. The three models were: (I) a CUS model (CUS features only, plus any serological variables retained after selection); (II) a CEUS model (CUS + CEUS features, plus any retained serological variables); and (III) a combined model (CUS + CEUS + MRI features, plus any retained serological variables). After selection, the final combined model retained seven imaging predictors: the CUS-derived tumor number, diameter, Adler blood flow grading and visualized macrovasculature around the tumor; the CEUS-derived arterial peritumoral enhancement and non-enhancing area; and the MRI-derived non-nodular

**Table 1** Univariate and multivariable analyses of preoperative clinical and imaging features in the prediction of histopathological findings

Clinical and radiological characteristics	Univariate analysis		Multivariate analysis	
	OR [95% CI]	P	OR [95% CI]	P
Sex	2.64 [0.96–9.33]	0.09		
Age	0.97 [0.94–1.01]	0.10		
Pathological type	6.05 [1.14–44.72]	0.04		
PLR	1.00 [1.00–1.01]	0.07		
ALT	3.13 [1.54–6.37]	0.002	CUS: 1.01 [1.00–1.01] <sup>1</sup>	CUS: 0.05 <sup>1</sup>
AST	2.43 [1.15–5.07]	0.02		
GGT	1.85 [0.92–3.86]	0.09		
Tumor number	3.81 [0.97–16.02]	0.05	CEUS: 4.92 [0.78–31.48] <sup>2</sup>	CEUS: 0.09 <sup>2</sup>
			Com: 33.76 [2.79–494.04] <sup>3</sup>	Com: 0.006 <sup>3</sup>
Diameter	1.20 [1.07–1.36]	0.003	Com: 0.73 [0.52–1.00] <sup>3</sup>	Com: 0.06 <sup>3</sup>
Capsule	2.59 [1.13–5.85]	0.02		
Adler blood flow grading	1.69 [1.26–2.29]	<0.001	CUS: 1.78 [1.18–2.71] <sup>1</sup>	CUS: 0.01 <sup>1</sup>
			CEUS: 1.72 [1.12–2.68] <sup>2</sup>	CEUS: 0.01 <sup>2</sup>
			Com: 3.24 [1.71–6.99] <sup>3</sup>	Com: <0.001 <sup>3</sup>
Visualized macrovasculature around the tumor	22.19 [6.88–99.77]	<0.001	CUS: 31.89 [8.16–171.33] <sup>1</sup>	CUS: <0.001 <sup>1</sup>
			CEUS: 41.00 [9.82–237.48] <sup>2</sup>	CEUS: <0.001 <sup>2</sup>
			Com: 137.29 [17.12–1,988.90] <sup>3</sup>	Com: <0.001 <sup>3</sup>
Arterial peritumoral enhancement	4.74 [1.79–13.10]	0.002	CEUS: 4.59 [1.15–18.43] <sup>2</sup>	CEUS: 0.03 <sup>2</sup>
			Com: 7.90 [1.25–57.43] <sup>3</sup>	Com: 0.03 <sup>3</sup>
Nonenhancing area	2.43 [1.15–5.07]	0.02	Com: 5.47 [1.02–36.73] <sup>3</sup>	Com: 0.06 <sup>3</sup>
Marked washout	5.02 [1.88–17.47]	0.004		
Non-nodular type tumor	18.62 [8.00–49.28]	<0.001	Com: 103.37 [19.64–896.55] <sup>3</sup>	Com: <0.001 <sup>3</sup>
Signal intensity	3.39 [1.70–7.02]	<0.001		

<sup>1</sup> = CUS model; <sup>2</sup> = CEUS model; <sup>3</sup> = Combined model (CUS + CEUS + MR features, with retained serologic covariates as applicable). ALT, alanine aminotransferase; AST, aspartate aminotransferase; CEUS, contrast-enhanced ultrasound; CI, confidence interval; Com, combined model (CUS + CEUS + MR features, with retained serologic covariates as applicable); CUS, conventional ultrasound; GGT, gamma-glutamyl transferase; MR, magnetic resonance; OR, odds ratio; PLR, platelet-to-lymphocyte ratio.

tumor type (AUC =0.937 in the modeling cohort; AUC =0.932 in external validation; *Tables 1,2*).

### Development and external validation for the MVI-prediction nomogram

For clarity, AUC1, AUC2, and AUC3 denote the ROC area under the curve in the modeling cohort for the CUS, CEUS, and the combined model, respectively. Accordingly, the modeling AUCs were AUC1=0.793, AUC2=0.838, and

AUC3=0.937. In the validation cohort, the AUCs were 0.816, 0.860, and 0.932, respectively. The DeLong test indicated a significant difference between the AUCs of the models (AUC3 *vs.* AUC2 *vs.* AUC1;  $P<0.05$ ; respectively) (*Figure 2A-2D*). The sensitivity, specificity, PPV, and NPV of each model are shown in *Table 2*.

We developed a nomogram for the combined model to estimate the risk of MVI based on the individual variables of multimodal imaging and serological signatures, including tumor number, diameter, Adler blood flow grading, visualized

**Table 2** Predictive performance of the CUS model, CEUS model, combination model, and extra model

Model	AUC, C-index [95% CI]	Sensitivity	Specificity	Accuracy	PPV	NPV
CUS model						
Modeling cohort (n=179)	0.793 [0.711–0.874]	0.40	0.97	0.82	0.83	0.82
Validation cohort (n=80)	0.816 [0.721–0.911]	0.78	0.74	0.76	0.72	0.80
Model CEUS						
Modeling cohort (n=179)	0.838 [0.773–0.901]	0.40	0.94	0.80	0.70	0.82
Validation cohort (n=80)	0.860 [0.779–0.941]	0.86	0.72	0.79	0.73	0.86
Com						
Modeling cohort (n=179)	0.937 [0.902–0.972]	0.72	0.94	0.88	0.81	0.91
Validation cohort (n=80)	0.932 [0.881–0.983]	0.84	0.84	0.84	0.82	0.86
Extra model						
Modeling cohort (n=179)	0.848 [0.778–0.918]	0.53	0.94	0.83	0.76	0.85
Validation cohort (n=80)	0.838 [0.746–0.930]	0.70	0.81	0.76	0.76	0.76

AFP, alpha-fetoprotein; AUC, area under the ROC curve; CEUS, contrast-enhanced ultrasound; CI, confidence interval; C-index, concordance index; Com, combined model (CUS + CEUS + MR features, with retained serologic covariates as applicable); CUS, conventional ultrasound; Extra model, comprising AFP, tumor number, tumor diameter, arterial peritumoral enhancement, and non-nodular tumor type; MR, magnetic resonance; NPV, negative predictive value; PPV, positive predictive value; ROC, receiver operating characteristic.

macrovasculature around the tumor, arterial peritumoral enhancement, nonenhancing area, and non-nodular type tumor (Figure 2A). We further subjected the combined model to bootstrap validation, with a bootstrap-corrected concordance index (C-index) of 0.937 (Figure 2B,2C). In addition, calibration plots indicated good agreement between the nomogram and histopathology of surgical specimens regarding the estimation of MVI risk; moreover, the decision curves showed that the net benefit of the nomogram was higher than that of assuming all patients have MVI.

Using the independent cohort from institution two, the nomogram based on the combined model maintained high discrimination for estimating the preoperative probability of MVI, with a C-index/ROC AUC =0.932 (95% CI, 0.88–0.98). For comparison, the CUS and CEUS models achieved AUC1 =0.816 and AUC2 =0.860, respectively (AUC1 denotes CUS; AUC2 denotes CEUS); DeLong tests showed that the combined model significantly outperformed both (P<0.05) (Figure 2D). Calibration—assessing the agreement between nomogram-predicted MVI probabilities and observed MVI frequencies—demonstrated good concordance in the validation cohort (Figure 3A,3B). DCA indicated a higher net benefit for the nomogram than treat-all or treat-none strategies across clinically relevant

threshold probabilities (Figure 3C,3D).

*Comparison of the combined model and the extra model*

As predefined in the Methods, the extra model incorporated AFP, tumor number, tumor diameter, arterial peritumoral enhancement, and non-nodular tumor type (22,25–28). Compared with the prespecified extra model (AUC 0.848 in the modeling cohort; 0.838 in external validation), the combined model showed superior discrimination in both cohorts (AUC 0.937 and 0.932, respectively; DeLong P<0.05 for each comparison). Calibration demonstrated close agreement between nomogram-predicted MVI probabilities and observed MVI frequencies, and DCA indicated a higher net benefit for the combined model than treat-all or treat-none across clinically relevant thresholds (Figure 4). According to these results, the combined model consistently outperformed the other models (the CUS, CEUS, and the extra models).

**Discussion**

This study established and validated a nomogram that integrated multimodal imaging and serological signatures to predict preoperative MVI in patients with HCC. After



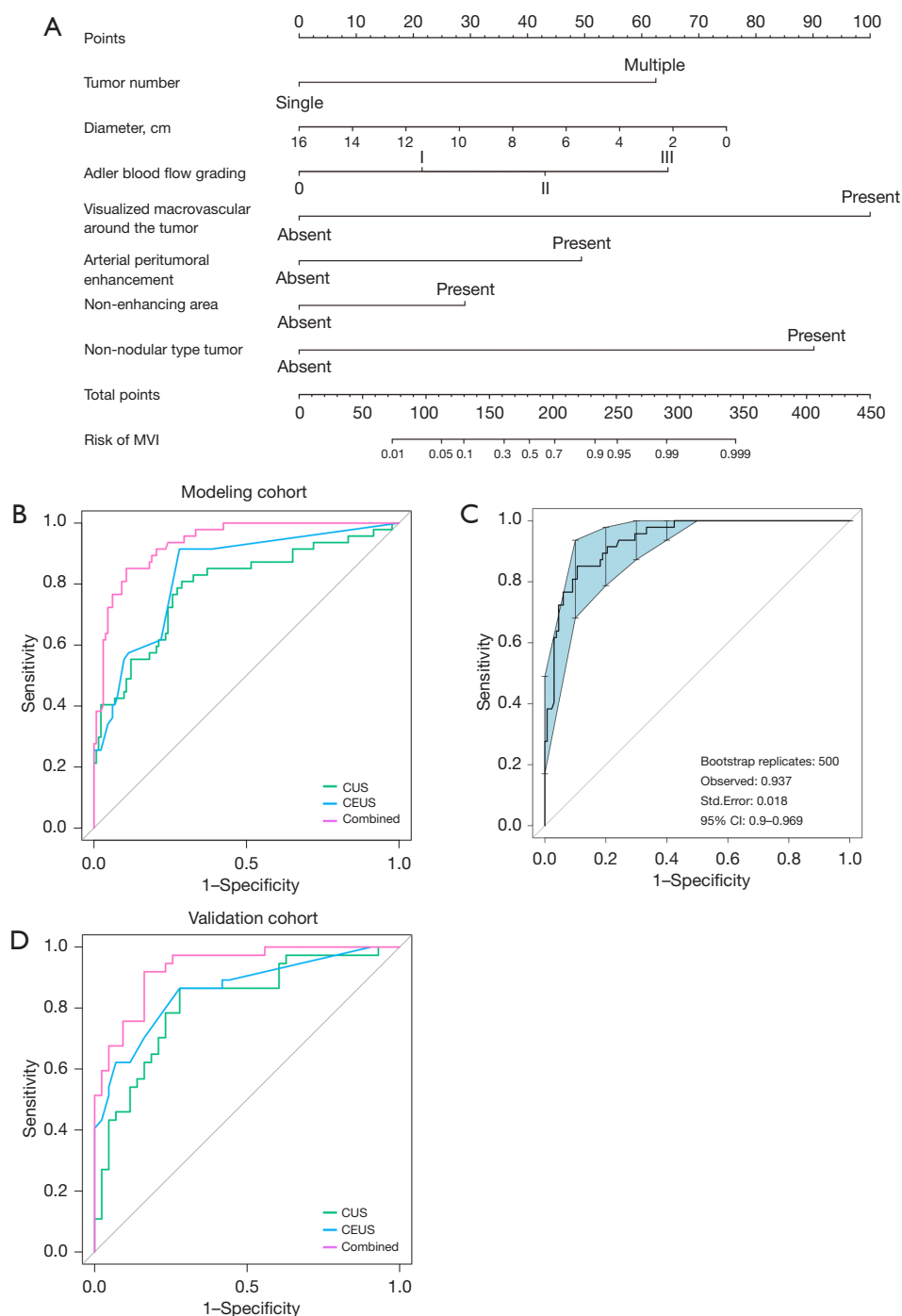


**Figure 2** Performance of the nomogram. (A) Nomogram for preoperative prediction of MVI in HCC. (B) ROC curve of the nomogram in the modeling cohort for the combined (0.937), CUS (0.793), and CEUS (0.838) models. (C) The bootstrap-corrected concordance index (AUC = 0.937; 95% CI: 0.9–0.969). (D) ROC curve of the nomogram in the validation cohort for the combined (0.932), CUS (0.816), and CEUS (0.860) models. Tumor diameter demonstrated an inverse relationship with MVI (OR = 0.73) and was retained for its clinical relevance. Although larger tumors are traditionally associated with MVI, emerging evidence suggests that fibrous encapsulation or necrosis in larger tumors may reduce MVI risk, whereas small, aggressive tumors may exhibit high vascular invasion potential. AUC, area under the curve; CEUS, contrast-enhanced ultrasound; CI, confidence interval; CUS, conventional ultrasound; HCC, hepatocellular carcinoma; MVI, microvascular invasion; OR, odds ratio; ROC, receiver operating characteristic; Std., standard.

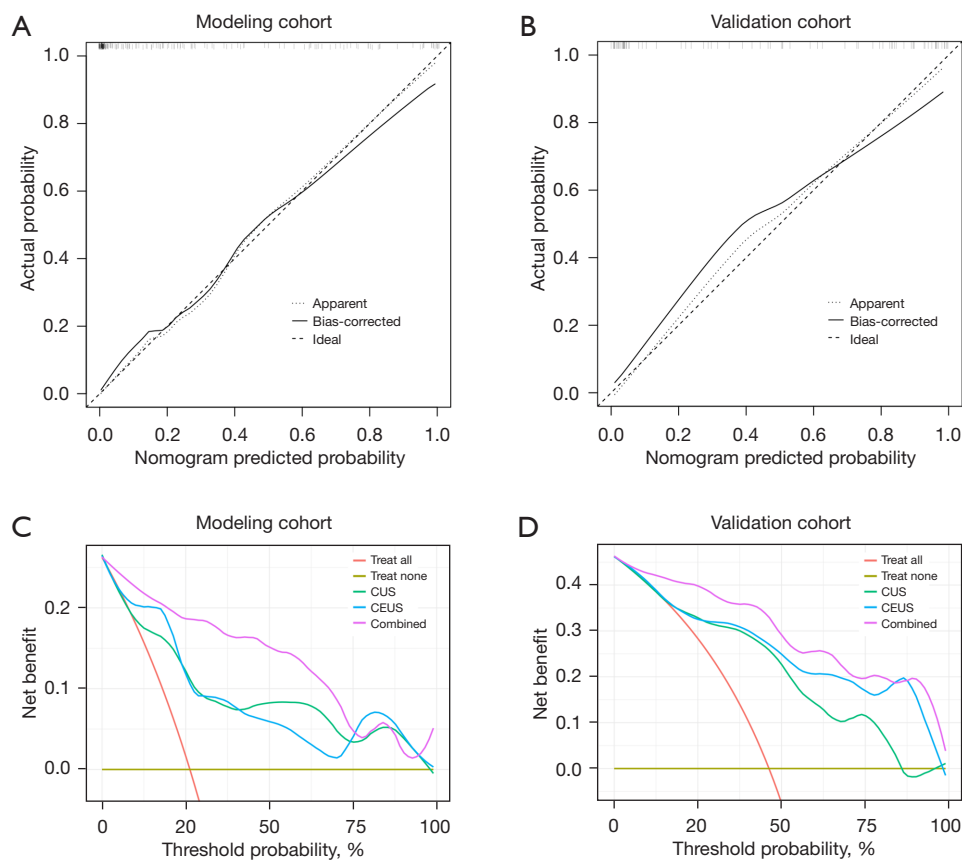


**Figure 3** Calibration curves in the (A) modeling cohort and (B) validation cohort and DCA in (C) the modeling cohort and (D) validation cohort. CEUS, contrast-enhanced ultrasound; CUS, conventional ultrasound; DCA, decision-curve analysis.

an independent external verification, the nomogram demonstrated good calibration, discrimination, and classification performance in both the modeling and validation cohorts. Interestingly, radiologists and surgeons could predict the presence of MVI in HCC with the help of our new model.

Imaging is playing an increasingly important role in the preoperative prediction of MVI. Although pathological confirmation remains the gold standard, imaging allows for the noninvasive, repeatable, and dynamic assessment of vascular invasion risk before treatment. Specific imaging features—such as nonsmooth tumor margins, peritumoral arterial enhancement, and macrovascular structures surrounding the tumor—have demonstrated strong correlations with MVI in HCC. These findings support the use of imaging as one of the most essential tools in early diagnostic and therapeutic decision-making. Therefore, our study focused on developing a multimodal

imaging-based prediction model to facilitate individualized management and improve outcomes in patients with HCC. These findings align with recent perspectives emphasizing preoperative MVI risk stratification to inform individualized therapy (e.g., Wang *et al.*) (29).

Our study investigated the predictive value of multimodal imaging for MVI in HCC. The final nomogram included radiological features from CUS, CEUS, and MR images and had higher AUCs of 0.937 and 0.932 in the modeling and validation cohorts, respectively, as compared to the model with CUS alone (modeling AUC =0.793; validation AUC =0.816) or that with CUS and CEUS (modeling AUC =0.838; validation AUC =0.860) ( $P<0.05$ ).

Our results indicated that tumor number, diameter, Adler blood flow grading, visualized macrovascularity around the tumor, arterial peritumoral enhancement, nonenhancing area, and non-nodular type tumor were significantly associated with MVI. This in line with studies reporting

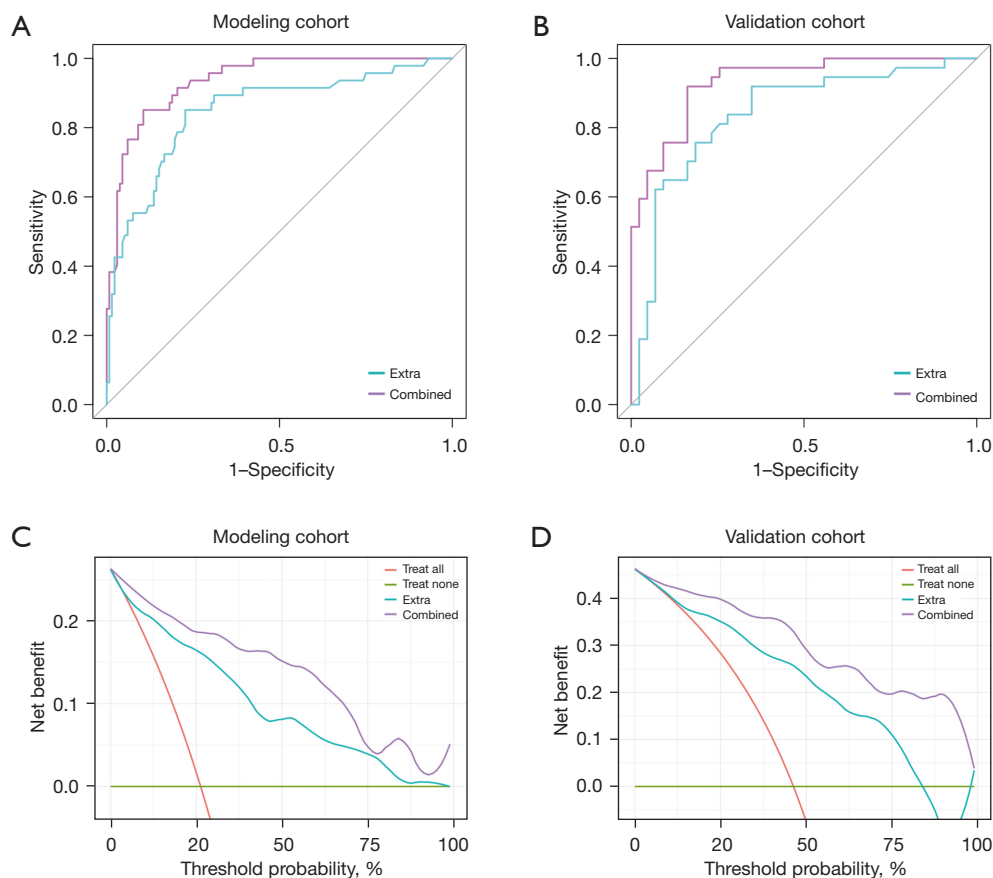


**Figure 4** Performance of the nomogram and the extra model. (A) ROC curve of nomogram and extra model in the modeling cohort (AUC: 0.937 vs. 0.848). (B) ROC curve of the nomogram and extra model in the validation cohort (AUC: 0.932 vs. 0.838). (C) DCA in the modeling cohort. (D) DCA in the validation cohort. The extra model (benchmark comparator) comprises AFP, tumor number, tumor diameter, arterial peritumoral enhancement, and non-nodular tumor type. AFP, alpha-fetoprotein; AUC, area under the ROC curve; DCA, decision-curve analysis; ROC, receiver operating characteristic.

that tumor number, tumor size, non-nodular type, and arterial peritumoral enhancement are highly predictive of histological MVI (15,30–35).

The mechanism underlying arterial peritumoral enhancement's correlation with MVI is likely compensatory arterial hyperperfusion leading to hemodynamic perfusion changes (36). This usually occurs in areas of decreased portal flow due to occlusion of minute portal branches by tumor thrombi, and the draining veins of encapsulated HCCs are typically portal venules. According to Kim *et al.* (27), the same pattern can be detected in gadolinium ethoxy benzyl diethylenetriamine pentaacetic acid (Gd-EOB-DTPA) MRI, including hepatobiliary phase images, and is a risk factor for MVI. A study by Nishie *et al.* (35) also demonstrated that marked peritumoral enhancement on both CT hepatic arteriography and CT aortoportography is

a significant predictor of MVI (in our study, the peritumoral enhancement data on CEUS were examined). They achieved satisfactory results, suggesting that it is possible to assess peritumoral enhancement using noninvasive techniques, such as CT, dynamic MRI, or CEUS, which are recommended for HCC diagnosis.

In our study, CEUS was used to identify qualitative enhancement patterns relevant to MVI risk. Although quantitative CEUS perfusion parameters, such as time-intensity curve (TIC) analysis or mean transit time, have been reported to correlate with tumor aggressiveness and MVI, we did not incorporate these parameters. This was due to the retrospective nature of our study and the lack of standardized perfusion acquisition tools across ultrasound systems in both institutions. Thus, robust and reproducible CEUS features—such as nonenhancing areas and

peritumoral enhancement—were prioritized in our model. Future prospective studies with uniform CEUS platforms and software should be conducted to investigate the added value of quantitative perfusion analysis.

On CEUS, the nonenhancing area within the tumor reflects necrosis and hypoxia. Several studies have demonstrated that hypoxia and necrosis can activate the aggressiveness of HCC or cause irregular rim-like arterial phase enhancement in the tumor (37–39). As a result, the presence of a nonenhancing area on CEUS may be an indicator of MVI risk. However, in our study, the nonenhancing area was included as a binary variable (present or absent), with no quantification of its actual size or proportion. This was due to limitations in standardizing CEUS image resolution and the absence of postprocessing tools in the retrospective setting. Future prospective studies may benefit from volumetric analysis of necrotic regions to further enhance the predictive performance of CEUS-based models.

Compared with purely intratumoral morphologic features (e.g., size, capsule) or intratumoral vascular signs, peritumoral microvascular markers within ~1 cm of the tumor margin—including high Adler blood-flow grade, visualized peritumoral macrovasculature, and arterial peritumoral enhancement—are more directly influenced by MVI and therefore exhibited stronger associations with histologic MVI in our cohorts. Therefore, we also focused on features around the tumor. Among these predictors, Adler blood-flow grading and visualized peritumoral macrovasculature have been less commonly incorporated into MVI prediction models; however, in our study, they showed a greater relative contribution to MVI prediction, as reflected by higher point assignments in the nomogram (and larger regression coefficients). They may help predict MVI due to the following: during MVI, tumor cell clusters are shed into the visualized draining vessels around the tumor (usually the peritumoral portal vein) (40), and some of these clusters may adhere to or even invade the blood vessel wall, obstructing and slowing blood flow microcirculation in the peritumoral drainage system.

Large tumor size has historically been considered to be a reliable predictor of MVI in HCC (15,30,31). However, emerging evidence and our findings suggest that tumor size alone may not be sufficient for prediction. Based on the *de novo* development hypothesis, HCCs  $\leq 2$  cm have also been associated with MVI and poor prognosis (41). Furthermore, it has been hypothesized that large tumors may undergo encapsulation or necrosis, thereby reducing peripheral vascular invasion (42,43). Conversely, small but

poorly differentiated tumors may pose a higher MVI risk. In our study, compared with non-vascular intratumoral morphologic features—particularly tumor diameter, which showed only a borderline association with MVI [odds ratio (OR) = 0.73; 95% CI: 0.52–1.00;  $P=0.063$ ]—peritumoral vascular features such as high Adler blood-flow grading and visualized peritumoral macrovasculature exhibited stronger and independent associations with MVI, underscoring the need for multiparametric imaging-based prediction models.

To further advance preoperative risk stratification for MVI, we constructed a multimodal nomogram that integrated grayscale ultrasound (CUS), CEUS, and gadoteric acid-enhanced MRI, along with serological markers. Previous studies have typically focused on single imaging modalities or lacked external validation, potentially limiting generalizability. In contrast, our approach combined complementary information from three imaging techniques and included an independent external validation cohort to assess reproducibility. Furthermore, we employed qualitative imaging features that are routinely available in clinical practice, increasing their translational potential. These elements distinguish our work and may provide a practical and individualized tool for preoperative MVI prediction in patients with HCC.

Furthermore, previous studies (22,25–28) have proposed several “worrisome” variables (e.g., AFP, tumor number, diameter, arterial peritumoral enhancement, and non-nodular type tumor) as predictors of MVI. However, these have not been widely recognized in the preoperative radiologic diagnosis of MVI in HCC. Consequently, we constructed an extra model incorporating these variables. Compared with the prespecified extra model (AUC = 0.848 in the modeling cohort; 0.838 in external validation), the combined model showed higher discrimination in the external validation cohort (AUC = 0.932); the difference was confirmed by DeLong tests ( $P<0.05$ ). DCA also demonstrated greater net benefit for the combined model than treat-all or treat-none across clinically relevant threshold probabilities.

Despite these promising results, this study involved several limitations that should be acknowledged. First, due to the retrospective design, the cohort recruitment might have been biased by the selection of surgical procedures, which might have led to an incomplete representation of all radiologic features of HCC. Second, the study lacked prospective validation, and thus, a prospective multicenter study is needed to verify our results. Third, the external validation cohort had a relatively small sample size. As part of future analyses, we will collect extracellular contrast

data and increase the sample size for validation. Moreover, contrast-enhanced CT was not included in our model due to its nonstandardized use across cohorts, and our aim was to develop a nonionizing and dynamically assessable multimodal model combining CUS, CEUS, and MRI. However, we acknowledge that the inclusion of contrast-enhanced CT in future models may offer further insights and improve generalizability. Finally, as ultrasound and CEUS are inherently operator-dependent modalities, variations in scanning technique and interpretation across operators or institutions may reduce the study's reproducibility. Although we used standardized protocols and experienced readers to minimize bias, this limitation should be considered in the broader application of our model in clinical practice.

## Conclusions

We developed a reliable combined model for the preoperative prediction of MVI in HCC that was highly accurate, specific, and sensitive. Clinical practitioners may benefit from this model based on the combination of CUS, CEUS, MRI, and serological signatures of HCC, as it can assist in optimizing interventions and achieving greater precision and individualization of treatment.

## Acknowledgments

None.

## Footnote

**Reporting Checklist:** The authors have completed the TRIPOD reporting checklist. Available at <https://qims.amegroups.com/article/view/10.21037/qims-2025-231/rc>

**Data Sharing Statement:** Available at <https://qims.amegroups.com/article/view/10.21037/qims-2025-231/dss>

**Funding:** This study was funded by the National Key Research and Development Program (No. 2020YFA0713800), Clinical Research Special Funding Program (No. 2022-LCYJ-MS-24), National Natural Science Foundation of China (Grant No. 82272013) and Clinical Research Plan of SHDC (Grant No. SHDC2020CR1031B).

**Conflicts of Interest:** All authors have completed the ICMJE

uniform disclosure form (available at <https://qims.amegroups.com/article/view/10.21037/qims-2025-231/coif>). The authors have no conflicts of interest to declare.

**Ethical Statement:** The authors are accountable for all aspects of the work in ensuring that questions related to the accuracy or integrity of any part of the work are appropriately investigated and resolved. Ethics approval was obtained from the Institutional Review Board of Nanjing Drum Tower Hospital, Affiliated Hospital of Medical School, Nanjing University (No. 2022-140-01), with informed consent waived owing to the retrospective design. Zhongshan Hospital, Fudan University, was informed and agreed to the study in accordance with institutional policy. This study was conducted in accordance with the Declaration of Helsinki and its subsequent amendments.

**Open Access Statement:** This is an Open Access article distributed in accordance with the Creative Commons Attribution-NonCommercial-NoDerivs 4.0 International License (CC BY-NC-ND 4.0), which permits the non-commercial replication and distribution of the article with the strict proviso that no changes or edits are made and the original work is properly cited (including links to both the formal publication through the relevant DOI and the license). See: <https://creativecommons.org/licenses/by-nc-nd/4.0/>.

## References

1. Siegel RL, Miller KD, Fuchs HE, Jemal A. Cancer statistics, 2022. *CA Cancer J Clin* 2022;72:7-33.
2. Kanwal F, Befeler A, Chari RS, Marrero J, Kahn J, Afdhal N, Morgan T, Roberts L, Mohanty SR, Schwartz J, VanThiel D, Li J, Zeringue A, Di'Bisceglie A. Potentially curative treatment in patients with hepatocellular cancer—results from the liver cancer research network. *Aliment Pharmacol Ther* 2012;36:257-65.
3. Tabrizian P, Jibara G, Shrager B, Schwartz M, Roayaie S. Recurrence of hepatocellular cancer after resection: patterns, treatments, and prognosis. *Ann Surg* 2015;261:947-55.
4. Lim KC, Chow PK, Allen JC, Chia GS, Lim M, Cheow PC, Chung AY, Ooi LL, Tan SB. Microvascular invasion is a better predictor of tumor recurrence and overall survival following surgical resection for hepatocellular carcinoma compared to the Milan criteria. *Ann Surg* 2011;254:108-13.
5. Erstad DJ, Tanabe KK. Prognostic and Therapeutic Implications of Microvascular Invasion in Hepatocellular



- Carcinoma. *Ann Surg Oncol* 2019;26:1474-93.
6. Shah SA, Cleary SP, Wei AC, Yang I, Taylor BR, Hemming AW, Langer B, Grant DR, Greig PD, Gallinger S. Recurrence after liver resection for hepatocellular carcinoma: risk factors, treatment, and outcomes. *Surgery* 2007;141:330-9.
7. Orcutt ST, Anaya DA. Liver Resection and Surgical Strategies for Management of Primary Liver Cancer. *Cancer Control* 2018;25:1073274817744621.
8. Roayaie S, Obeidat K, Sposito C, Mariani L, Bhoori S, Pellegrinelli A, Labow D, Llovet JM, Schwartz M, Mazzaferro V. Resection of hepatocellular cancer  $\leq 2$  cm: results from two Western centers. *Hepatology* 2013;57:1426-35.
9. Han J, Li ZL, Xing H, Wu H, Zhu P, Lau WY, Zhou YH, Gu WM, Wang H, Chen TH, Zeng YY, Wu MC, Shen F, Yang T. The impact of resection margin and microvascular invasion on long-term prognosis after curative resection of hepatocellular carcinoma: a multi-institutional study. *HPB (Oxford)* 2019;21:962-71.
10. Rodríguez-Perálvarez M, Luong TV, Andreana L, Meyer T, Dhillon AP, Burroughs AK. A systematic review of microvascular invasion in hepatocellular carcinoma: diagnostic and prognostic variability. *Ann Surg Oncol* 2013;20:325-39.
11. Rungsakulkij N, Mingphruedhi S, Suragul W, Tangtawee P, Muangkaew P, Aeesoa S. Platelet-to-Lymphocyte Ratio and Large Tumor Size Predict Microvascular Invasion after Resection for Hepatocellular Carcinoma. *Asian Pac J Cancer Prev* 2018;19:3435-41.
12. Zhu Y, Xu D, Zhang Z, Dong J, Zhou Y, Zhang WW, Hong L, Zhu WW. A new laboratory-based algorithm to predict microvascular invasion and survival in patients with hepatocellular carcinoma. *Int J Surg* 2018;57:45-53.
13. Levi Sandri GB, Spoleitini G, Vennarecci G, Francone E, Abu Hilal M, Ettorre GM. Laparoscopic liver resection for large HCC: short- and long-term outcomes in relation to tumor size. *Surg Endosc* 2018;32:4772-9.
14. Nishie A, Yoshimitsu K, Irie H, Tajima T, Hirakawa M, Ishigami K, Ushijima Y, Okamoto D, Nishihara Y, Taketomi A, Honda H. Radiological detectability of minute hepatic venous invasion in hepatocellular carcinoma. *Eur J Radiol* 2009;70:517-24.
15. Renzulli M, Brocchi S, Cucchetti A, Mazzotti F, Mosconi C, Sportoletti C, Brandi G, Pinna AD, Golfieri R. Can Current Preoperative Imaging Be Used to Detect Microvascular Invasion of Hepatocellular Carcinoma? *Radiology* 2016;279:432-42.
16. Chandarana H, Robinson E, Hajdu CH, Drozhinin L, Babb JS, Taouli B. Microvascular invasion in hepatocellular carcinoma: is it predictable with pretransplant MRI? *AJR Am J Roentgenol* 2011;196:1083-9.
17. Dong Y, Qiu Y, Yang D, Yu L, Zuo D, Zhang Q, Tian X, Wang WP, Jung EM. Potential application of dynamic contrast enhanced ultrasound in predicting microvascular invasion of hepatocellular carcinoma. *Clin Hemorheol Microcirc* 2021;77:461-9.
18. Forner A, Reig M, Bruix J. Hepatocellular carcinoma. *Lancet* 2018;391:1301-14.
19. Wildner D, Schellhaas B, Strack D, Goertz RS, Pfeifer L, Fiessler C, Neurath MF, Strobel D. Differentiation of malignant liver tumors by software-based perfusion quantification with dynamic contrast-enhanced ultrasound (DCEUS). *Clin Hemorheol Microcirc* 2019;71:39-51.
20. Schwarze V, Marschner C, Völckers W, de Figueiredo GN, Rübenthaler J, Clevert DA. The diagnostic performance of contrast-enhanced ultrasound (CEUS) for evaluating hepatocellular carcinoma (HCC) juxtaposed to MRI findings; a retrospective single-center analysis of 292 patients. *Clin Hemorheol Microcirc* 2020;76:155-60.
21. Sidhu PS, Cantisani V, Dietrich CF, Gilja OH, Saftoiu A, Bartels E, et al. The EFSUMB Guidelines and Recommendations for the Clinical Practice of Contrast-Enhanced Ultrasound (CEUS) in Non-Hepatic Applications: Update 2017 (Long Version). *Ultraschall Med* 2018;39:e2-e44.
22. Wang WT, Yang L, Yang ZX, Hu XX, Ding Y, Yan X, Fu CX, Grimm R, Zeng MS, Rao SX. Assessment of Microvascular Invasion of Hepatocellular Carcinoma with Diffusion Kurtosis Imaging. *Radiology* 2018;286:571-80.
23. Adler DD, Carson PL, Rubin JM, Quinn-Reid D. Doppler ultrasound color flow imaging in the study of breast cancer: preliminary findings. *Ultrasound Med Biol* 1990;16:553-9.
24. Kang I, Jang M, Lee JG, Han DH, Joo DJ, Kim KS, Kim MS, Choi JS, Kim SI, Park YN, Choi GH. Subclassification of Microscopic Vascular Invasion in Hepatocellular Carcinoma. *Ann Surg* 2021;274:e1170-8.
25. Lei Z, Li J, Wu D, Xia Y, Wang Q, Si A, Wang K, Wan X, Lau WY, Wu M, Shen F. Nomogram for Preoperative Estimation of Microvascular Invasion Risk in Hepatitis B Virus-Related Hepatocellular Carcinoma Within the Milan Criteria. *JAMA Surg* 2016;151:356-63.
26. Banerjee S, Wang DS, Kim HJ, Sirlin CB, Chan MG, Korn RL, Rutman AM, Siripongsakun S, Lu D, Imanbayev G, Kuo MD. A computed tomography radiogenomic

- biomarker predicts microvascular invasion and clinical outcomes in hepatocellular carcinoma. *Hepatology* 2015;62:792-800.
27. Kim H, Park MS, Choi JY, Park YN, Kim MJ, Kim KS, Choi JS, Han KH, Kim E, Kim KW. Can microvessel invasion of hepatocellular carcinoma be predicted by pre-operative MRI? *Eur Radiol* 2009;19:1744-51.
  28. Poté N, Cauchy F, Albuquerque M, Voitot H, Belghiti J, Castera L, Puy H, Bedossa P, Paradis V. Performance of PIVKA-II for early hepatocellular carcinoma diagnosis and prediction of microvascular invasion. *J Hepatol* 2015;62:848-54.
  29. Wang F, Liao HZ, Chen XL, Lei H, Luo GH, Chen GD, Zhao H. Preoperative prediction of microvascular invasion: new insights into personalized therapy for early-stage hepatocellular carcinoma. *Quant Imaging Med Surg* 2024;14:5205-23.
  30. Kim SJ, Lee KK, Kim DG. Tumor size predicts the biological behavior and influence of operative modalities in hepatocellular carcinoma. *Hepatogastroenterology* 2010;57:121-6.
  31. Ma X, Wei J, Gu D, Zhu Y, Feng B, Liang M, Wang S, Zhao X, Tian J. Preoperative radiomics nomogram for microvascular invasion prediction in hepatocellular carcinoma using contrast-enhanced CT. *Eur Radiol* 2019;29:3595-605.
  32. Chou CT, Chen RC, Lin WC, Ko CJ, Chen CB, Chen YL. Prediction of microvascular invasion of hepatocellular carcinoma: preoperative CT and histopathologic correlation. *AJR Am J Roentgenol* 2014;203:W253-9.
  33. Xu X, Zhang HL, Liu QP, Sun SW, Zhang J, Zhu FP, Yang G, Yan X, Zhang YD, Liu XS. Radiomic analysis of contrast-enhanced CT predicts microvascular invasion and outcome in hepatocellular carcinoma. *J Hepatol* 2019;70:1133-44.
  34. Miyata R, Tanimoto A, Wakabayashi G, Shimazu M, Nakatsuka S, Mukai M, Kitajima M. Accuracy of preoperative prediction of microinvasion of portal vein in hepatocellular carcinoma using superparamagnetic iron oxide-enhanced magnetic resonance imaging and computed tomography during hepatic angiography. *J Gastroenterol* 2006;41:987-95.
  35. Nishie A, Yoshimitsu K, Asayama Y, Irie H, Tajima T, Hirakawa M, Ishigami K, Nakayama T, Kakihara D, Nishihara Y, Taketomi A, Honda H. Radiologic detectability of minute portal venous invasion in hepatocellular carcinoma. *AJR Am J Roentgenol* 2008;190:81-7.
  36. Matsui O, Kobayashi S, Sanada J, Kouda W, Ryu Y, Kozaka K, Kitao A, Nakamura K, Gabata T. Hepatocellular nodules in liver cirrhosis: hemodynamic evaluation (angiography-assisted CT) with special reference to multi-step hepatocarcinogenesis. *Abdom Imaging* 2011;36:264-72.
  37. Liu L, Zhu XD, Wang WQ, Shen Y, Qin Y, Ren ZG, Sun HC, Tang ZY. Activation of beta-catenin by hypoxia in hepatocellular carcinoma contributes to enhanced metastatic potential and poor prognosis. *Clin Cancer Res* 2010;16:2740-50.
  38. Lequeux A, Noman MZ, Xiao M, Van Moer K, Hasmim M, Benoit A, Bosseler M, Viry E, Arakelian T, Berchem G, Chouaib S, Janji B. Targeting HIF-1 alpha transcriptional activity drives cytotoxic immune effector cells into melanoma and improves combination immunotherapy. *Oncogene* 2021;40:4725-35.
  39. Rhee H, An C, Kim HY, Yoo JE, Park YN, Kim MJ. Hepatocellular Carcinoma with Irregular Rim-Like Arterial Phase Hyperenhancement: More Aggressive Pathologic Features. *Liver Cancer* 2019;8:24-40.
  40. Fang JH, Zhou HC, Zhang C, Shang LR, Zhang L, Xu J, Zheng L, Yuan Y, Guo RP, Jia WH, Yun JP, Chen MS, Zhang Y, Zhuang SM. A novel vascular pattern promotes metastasis of hepatocellular carcinoma in an epithelial-mesenchymal transition-independent manner. *Hepatology* 2015;62:452-65.
  41. Theise ND, Marcelin K, Goldfischer M, Hytioglou P, Ferrell L, Thung SN. Low proliferative activity in macroregenerative nodules: evidence for an alternate hypothesis concerning human hepatocarcinogenesis. *Liver* 1996;16:134-9.
  42. Ng IO, Lai EC, Ng MM, Fan ST. Tumor encapsulation in hepatocellular carcinoma. A pathologic study of 189 cases. *Cancer* 1992;70:45-9.
  43. Feng Z, Li H, Zhao H, Jiang Y, Liu Q, Chen Q, Wang W, Rong P. Preoperative CT for Characterization of Aggressive Macrotrabecular-Massive Subtype and Vessels That Encapsulate Tumor Clusters Pattern in Hepatocellular Carcinoma. *Radiology* 2021;300:219-29.

**Cite this article as:** Wu J, Xu Y, Liu H, Wen B, Wang W, Kong W. A nomogram based on a combination of preoperative multimodal imaging and serological signatures for predicting microvascular invasion of hepatocellular carcinoma: an independent external validation study. *Quant Imaging Med Surg* 2025;15(11):11103-11117. doi: 10.21037/qims-2025-231